

# GaussianOcc3D: A Gaussian-Based Adaptive Multi-modal 3D Occupancy Prediction

A. Enes Doruk, and Hasan F. Ates

**Abstract**—3D semantic occupancy prediction is a pivotal task in autonomous driving, providing a dense and fine-grained understanding of the surrounding environment, yet single-modality methods face trade-offs between camera semantics and LiDAR geometry. Existing multi-modal frameworks often struggle with modality heterogeneity, spatial misalignment, and the representation crisis—where voxels are computationally heavy and BEV alternatives are lossy. We present GaussianOcc3D, a multi-modal framework bridging camera and LiDAR through a memory-efficient, continuous 3D Gaussian representation. We introduce four modules: (1) LiDAR Depth Feature Aggregation (LDFA), using depth-wise deformable sampling to lift sparse signals onto Gaussian primitives; (2) Entropy-Based Feature Smoothing (EBFS) to mitigate domain noise; (3) Adaptive Camera-LiDAR Fusion (ACLF) with uncertainty-aware reweighting for sensor reliability; and (4) a Gauss-Mamba Head leveraging Selective State Space Models for global context with linear complexity. Evaluations on Occ3D, SurroundOcc, and SemanticKITTI benchmarks demonstrate state-of-the-art performance, achieving mIoU scores of 49.4%, 28.9%, and 25.2% respectively. GaussianOcc3D exhibits superior robustness across challenging rainy and nighttime conditions. Code

**Index Terms**—3D Occupancy prediction, Gaussian representation, multi-modal learning.

## I. INTRODUCTION

The 3D semantic occupancy prediction is a pivotal task in the field of autonomous driving, providing a dense and fine-grained volumetric understanding of the surrounding environment [1], [2]. Unlike traditional 3D object detection tasks that predominantly focus on specific classes of foreground objects using discrete bounding boxes, semantic occupancy prediction requires a comprehensive perception of the scene by predicting the geometry and semantics of both occupied and free space [1], [2]. This capability is indispensable for navigating long-tail safety challenges, such as irregular roadway hazards, fallen rubble, or construction overhangs, which defy predefined rigid ontologies [1].

While recent advances have demonstrated significant progress in single-modality occupancy prediction. Camera-centric models, such as TPVFormer [3] and GaussianFormer [4], leverage photometric richness for semantic understanding but suffer from the ill-posed nature of depth estimation from 2D images. Conversely, LiDAR-based solutions like JS3C-Net [5] and LMSCNet [6] provide precise geometric manifolds but lack the fine-grained semantic information required to distinguish visually similar classes.

Multi-modal synergy seeks to resolve these ambiguities by leveraging the complementary strengths of both sensors. However, many existing multi-modal frameworks encounter significant difficulties in managing modality heterogeneity, spatial

misalignment, and insufficient sensor interactions, which can result in the loss of critical semantic or geometric cues. These challenges are further compounded by a fundamental representation crisis in 3D perception: complex voxel-based models, such as OpenOccupancy [7], suffer from excessive computational demands due to the processing of empty space, while lightweight Bird’s-Eye View (BEV) alternatives often rely on lossy compression that fails to accurately represent vertical structures and height information.

The emergence of 3D Gaussian Splatting [4] has offered a continuous, memory-efficient alternative for environmental representation, notably explored in camera-centric models like GaussianFormer [4], [8]. However, vision-only Gaussian approaches often struggle with spurious geometry induced by depth ambiguity and overlook the robust geometric priors encoded in LiDAR data. To address these gaps, we propose GaussianOcc3D, a novel framework that bridges camera semantics and LiDAR geometry within a unified, shared Gaussian space. Our primary motivation is to overcome the sparsity of LiDAR data and the uncertainty of camera depth by natively lifting multi-modal signals onto adaptive Gaussian primitives. By utilizing anisotropic Gaussians that fit directly onto object surfaces rather than discretizing empty space, our model avoids the redundant processing inherent in voxel-based systems while ensuring geometric-semantic consistency. Our contributions are summarized as follows:

- We propose GaussianOcc3D, a novel multi-modal occupancy prediction framework that bridges camera semantics and LiDAR geometry within a unified, memory-efficient 3D Gaussian representation.
- To address modality-specific challenges, we introduce the LiDAR Depth Feature Aggregation (LDFA) module for lifting sparse geometric signals via depth-wise deformable sampling, and the Entropy-Based Feature Smoothing (EBFS) module, which utilizes bidirectional cross-entropy to suppress inter-modal noise.
- We develop a dynamic Adaptive Camera-LiDAR Fusion (ACLF) mechanism featuring consistency-aware reweighting, alongside a Gauss-Mamba Head that leverages Selective State Space Models to capture long-range global context with linear complexity.
- Extensive evaluations on Occ3D, SurroundOcc, and SemanticKITTI benchmarks demonstrate state-of-the-art performance (e.g., 49.4% mIoU on Occ3D) and superior robustness in adverse weather and low-light conditions.

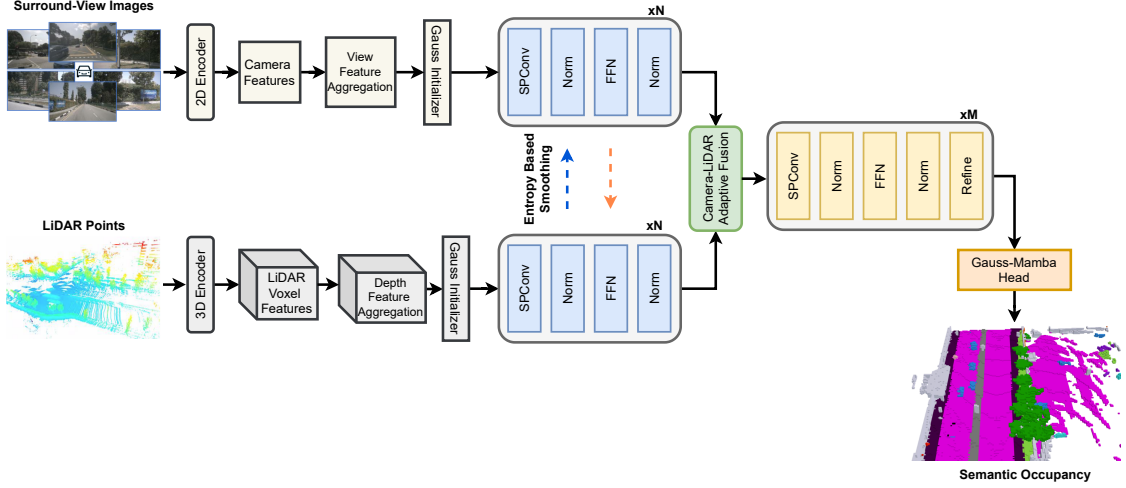


Fig. 1: The overall architecture of the proposed GaussianOcc3D framework.

## II. RELATED WORK

**3D Semantic Occupancy Prediction.** Recent research has transitioned from sparse 3D object detection toward dense semantic occupancy prediction to address long-tail safety challenges in autonomous driving [2]. Camera-based solutions aim to obtain voxel-level semantic information from monocular or multi-view images. Early successes like FB-OCC [9] utilized forward and backward view transformations, while OccDepth [10] integrated depth estimation to guide voxel assignments. More recent innovations include AdaOcc [11] for adaptive resolution. Despite these advances, vision-only methods remain limited by depth uncertainty. On the other hand, LiDAR-based models like S3CNet [5] and LMSCNet [6] focus on 3D convolutions in voxel space. Subsequent developments include PointOcc [12], which uses a cylindrical tri-perspective view. While geometrically accurate, these models often struggle with semantic ambiguity in areas like road-sidewalk boundaries.

**Multi-Modal Fusion Strategies.** LiDAR and camera sensors is essential for capitalizing on the complementary strengths of geometric precision and semantic richness [1].

1) Projection-based fusion paradigm [13], [14] combines image features with LiDAR points or projects point clouds into a range view to merge with photometric signals. 2) Feature-level fusion methods [15], [16] project both LiDAR and image data into a feature space, such as BEV or voxels, to learn cross-modal complementarities. 3) Attention-based fusion works [14], [3] utilize LiDAR features or spatial queries to sample image features through cross-attention mechanisms. Recent works like OccMamba [17] have explored Mamba to handle large-scale occupancy grids. However, our method diverges by leveraging a Gaussian representation to expand the semantic perception field with aligned geometric abstractions, reducing errors from inaccurate calibrations.

**3D Gaussian Splatting.** Gaussian Splatting [4] has emerged as a memory-efficient alternative to traditional voxelization. These methods model the scene as a collection of

anisotropic 3D Gaussians, concentrating computational resources on object surfaces rather than discretizing empty space, thus avoiding  $O(N^3)$  complexity. Within occupancy prediction, GaussianFormer [4] first established a query-centric paradigm to predict Gaussian parameters. Building on this, GaussianFormer-2 [8] proposed a probabilistic Gaussian superposition. While these are primarily camera-centric, our GaussianOcc3D leverages 3D Gaussians for both camera and LiDAR side, lifting multi-modal signals into a shared Gaussian space to maintain geometric and semantic consistency.

## III. METHOD

### A. Framework Overview

The architecture of GaussianOcc3D aims to unify multi-modal sensor streams within a continuous, memory-efficient 3D Gaussian representation. Given multi-view images  $\mathcal{I} = \{I_i\}_{i=1}^{N_c}$  and LiDAR point clouds  $\mathcal{P} = \{P_i\}_{i=1}^{N_p}$ , where  $P_i = (x_i, y_i, z_i, \eta_i)$  contains the 3D position and intensity, our goal is to predict a semantic occupancy grid  $\hat{O} \in \mathcal{C}^{X \times Y \times Z}$ . Unlike rigid voxel grids that suffer from cubic computational complexity, we model the scene as a set of 3D Gaussians  $\mathcal{G} = \{G_i\}_{i=1}^{N_g}$ . Each Gaussian  $G_i$  is parameterized by its mean  $m_i \in \mathbb{R}^3$ , rotation  $r_i \in \mathbb{R}^4$ , scale  $s_i \in \mathbb{R}^3$ , opacity  $\sigma_i \in [0, 1]$ , and a semantic logit vector  $c_i \in \mathbb{R}^{|C|}$  representing the class-wise scores.

The core principle of our representation is the universal approximation capability of Gaussian mixtures, which allows the model to adaptively fit anisotropic primitives to object surfaces. The semantic contribution of a single Gaussian evaluated at a location  $x$  is defined as:

$$g(x; G) = \sigma \cdot \exp \left( -\frac{1}{2} (x - m)^T \Sigma^{-1} (x - m) \right) \cdot c, \quad (1)$$

where  $\Sigma = RSS^T R^T$  represents the covariance matrix, with  $R$  and  $S$  being the rotation and scale matrices derived from  $r$  and  $s$ . To determine the occupancy and semantics of a specific voxel, we employ a Gaussian-to-voxel splatting

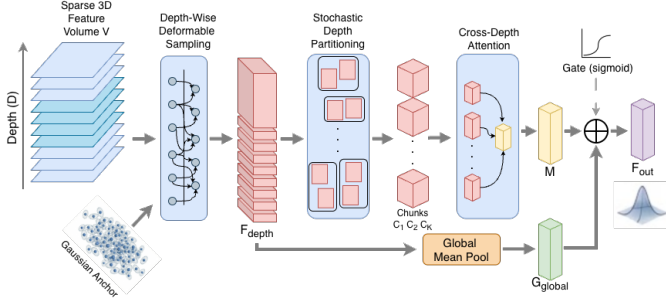


Fig. 2: Architecture of the LiDAR Depth Feature Aggregation Module.

module that aggregates these contributions within a localized radius. The resulting semantic feature vector  $\hat{o}(x)$  at the location  $x$  is calculated as follows:

$$\hat{o}(x; \mathcal{G}) = \sum_{i=1}^{N_g(x)} g_i(x; m_i, s_i, r_i, \sigma_i, c_i). \quad (2)$$

The final semantic label for each voxel is then determined by applying the  $\text{argmax}(\cdot)$  operator over the aggregated logit vector  $\hat{o}(x)$ .

As illustrated in Fig. 1, the pipeline operates by first extracting 2D features via a camera backbone and 3D geometric features via a sparse LiDAR backbone. After Gaussian initialization, we employ an encoder consisting of SPConv, normalization, and an FFN to process these features. These features are then lifted into the shared Gaussian space through a multi-modal feature aggregation, utilizing query-based multi-view fusion for images [4] and our proposed LDFA module for sparse LiDAR signals. Before merging the modalities, we employ an entropy-based feature smoothing module to ensure local consistency within the Gaussian descriptors. Subsequently, the ACLF module adaptively fuses these representations to prioritize reliable sensory data. After fusion, the representations are refined through SPConv, normalization, and FFN layers to ensure feature consistency. Finally, the fused features are refined by the Gauss-Mamba Head to capture global context for the final occupancy prediction. The framework is trained end-to-end using a joint objective function:

$$\mathcal{L}_{total} = \lambda_{ce} \mathcal{L}_{ce}(\hat{O}, \bar{O}) + \lambda_{lov} \mathcal{L}_{lov}(\hat{O}, \bar{O}), \quad (3)$$

where  $\mathcal{L}_{ce}$  is the cross-entropy loss and  $\mathcal{L}_{lov}$  is the Lovász-softmax loss [18] optimized against ground truth labels  $\bar{O}$ .

### B. Multi-Modal Feature Aggregation

Our architecture leverages a bifurcated processing stream to integrate dense photometric camera data and sparse geometric LiDAR data. For the camera branch, we adopt the multi-view aggregation paradigm of GaussianFormer [4], treating 3D Gaussian anchors as spatial queries. These anchors are defined as learnable 3D centroids  $\{a_i\}_{i=1}^{N_g}$  that serve as reference points to extract appearance features from surround-view images, ensuring photometric consistency across views.

The LiDAR branch utilizes a novel LiDAR Depth Feature Aggregation (LDFA) module. As illustrated in Fig. 2, we process the point cloud through a 3D sparse encoder to generate a voxelized feature volume  $V \in R^{C \times D \times H \times W}$ , where the vertical dimension is interpreted as a stack of  $D$  depth planes. We employ a depth-wise deformable sampling strategy [4] where learnable offsets generate  $P$  keypoints around each anchor. For an anchor  $i$  at depth plane  $d$ , the stratified feature  $f_{i,d}$  is computed as:

$$f_{i,d} = \sum_{k=1}^P w_{ik} \cdot P_d(u_{ik}), \quad (4)$$

where  $w_{ik}$  is the learnable attention weight for the  $k$ -th sampling point,  $u_{ik}$  represents the 2D projected coordinates of the keypoint on the  $d$ -th plane, and  $P_d(\cdot)$  denotes the bilinear interpolation operator applied to the feature map of that specific depth level.

To address sparsity and enhance robustness, we implement stochastic depth partitioning, inspired by the chunk-based processing in DA-Mamba [19]. We divide the  $D$  levels into  $K$  disjoint chunks. During training, we apply a random permutation  $\pi$  to the depth indices to prevent the model from overfitting to fixed spatial arrangements. The aggregated chunk representation  $C_k$  is derived via mean pooling:

$$C_k = \frac{1}{|S_k|} \sum_{d \in S_k} F_{depth}^{(\pi(d))}, \quad (5)$$

where  $S_k$  is the set of indices belonging to the  $k$ -th chunk and  $\pi(d)$  denotes the stochastic mapping of depth planes.

A cross-depth attention mechanism then generates a modulation vector  $M$  to identify valid surfaces by correlating chunk contexts. Finally, we re-introduce global context via a Gated Global Fusion mechanism, using a learnable soft gate  $\alpha \in [0, 1]$  to balance modulated signals with the global mean feature  $G_{global}$ :

$$\mathbf{F}_{out} = \alpha \cdot M + (1 - \alpha) \cdot G_{global}. \quad (6)$$

This LDFA module ensures that Gaussian primitives are initialized with features that are geometrically grounded, significantly improving the fidelity of the 3D occupancy prediction.

### C. Entropy-Based Feature Smoothing

The Entropy-Based Feature Smoothing (EBFS) module addresses the distributional misalignment that occurs when lifting camera and LiDAR features into a Gaussian space. Because images provide dense photometric texture while LiDAR provides sparse geometric manifolds, the resulting Gaussian feature descriptors often exhibit aliased distributions. This leads to the presence of characteristic rigid features that are non-transferable between modalities, where domain-specific sensor noise—such as visual glare or LiDAR multi-path reflections—corrupts the shared representation. EBFS quantifies uncertainty between streams via cross-entropy, dynamically rectifying the feature space to suppress these inconsistencies and artifacts before the fusion.

To ensure the framework learns intrinsically stable representations, we implement a stochastic execution strategy. Rather

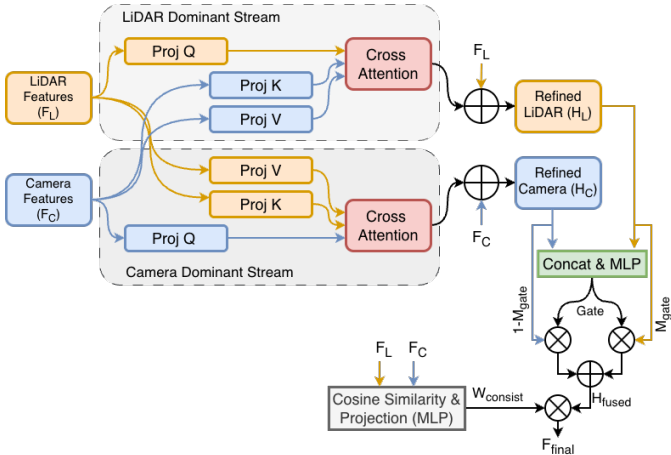


Fig. 3: Architecture of the Adaptive Camera-LiDAR Fusion Module.

than applying smoothing to every layer, we randomly select a subset of layers to undergo refinement during each training iteration [20]. This approach prevents the model from overrelying on the module to correct misalignments and serves as a regularization constraint that forces the encoder to produce robust camera and LiDAR features.

The core mechanism for quantifying sensor discrepancy is Cross-Entropy (CE). We interpret normalized feature vectors as probability distributions over the latent semantic space. Let  $F_C$  and  $F_L$  denote the camera and LiDAR feature sets. We convert raw logits into probability distributions  $P_C$  and  $Q_L$  using Softmax scaled by temperature  $\tau$ :

$$P_C = \text{Softmax} \left( \frac{F_C}{\tau} \right), \quad Q_L = \text{Softmax} \left( \frac{F_L}{\tau} \right) \quad (7)$$

To refine the fused representation, we implement a bidirectional cross-entropy mechanism to quantify the alignment between modalities. We calculate two distinct entropy maps: camera-dominant entropy ( $H_{C \rightarrow L}$ ), which measures LiDAR alignment with visual targets, and LiDAR-dominant entropy ( $H_{L \rightarrow C}$ ), which identifies visual ambiguity relative to geometric references:

$$H_{m \rightarrow n} = - \sum_{c=1}^C P_m^{(c)} \cdot \log \left( Q_n^{(c)} + \xi \right) \quad (8)$$

where  $(m, n) \in \{(C, L), (L, C)\}$ . These maps are transformed into modulation weights  $W_C$  and  $W_L$  via exponential decay, normalized by the sum  $\omega_{sum} = \sum \exp(-H) + \xi$ .

Finally, the features are updated via a residual connection with a learnable scaling parameter  $\epsilon$  to adaptively tune the refinement intensity during training:

$$\tilde{F}_i = F_i + \epsilon \cdot W_i, \quad i \in \{C, L\} \quad (9)$$

This smoothing process suppresses noise in conflicting regions while reinforcing semantically consistent structures, leading to sharper boundaries in the final prediction.

#### D. Adaptive Camera-LiDAR Fusion

To address the limitations of rigid sensor aggregation, we propose the Adaptive Camera-LiDAR Fusion (ACLF) module. This architecture treats fusion as a dynamic, context-aware process that explicitly models inter-modal consistency. Our approach is motivated by the fact that sensor reliability fluctuates per frame; for example, LiDAR may provide superior geometry in low-light conditions while the camera excels in capturing semantic boundaries during clear daylight, meaning no single modality is universally stable across all frames.

The process begins with dual-stream cross-attention refining modality-specific features  $F_L$  and  $F_C$  through cross-context. For the LiDAR-dominant stream, geometric queries  $Q_L$  seek semantic texture from camera keys  $K_C$  and values  $V_C$ :

$$H_L = F_L + \text{Softmax} \left( \frac{Q_L \cdot K_C^T}{\sqrt{d}} \right) V_C \quad (10)$$

Symmetrically, the camera-dominant stream  $H_C$  extracts structural context from the LiDAR features using queries  $Q_C$ .

To integrate these refined streams, we employ a soft gating mechanism. We project the concatenated features through a learned MLP to predict a fusion mask  $M_{gate} \in [0, 1]$ , allowing the network to adaptively weight sensor dominance:

$$H_{fused} = M_{gate} \odot H_L + (1 - M_{gate}) \odot H_C \quad (11)$$

Finally, to mitigate sensor conflict (e.g., visual hallucinations or LiDAR noise), we introduce a consistency-aware reweighting prior. This mechanism acts as a learned noise-suppression filter that utilizes the cosine similarity between projected camera and LiDAR latent spaces to quantify semantic consensus. Our motivation for using cosine similarity is to identify disagreements between sensors; a high similarity score indicates multi-modal agreement, while a low score signals potential hallucinations or domain-specific noise. By transforming this similarity into a channel-wise consistency gate  $W_{consist}$ , the model can adaptively suppress specific feature channels where sensors disagree—such as depth signals during a reflection—while preserving reliable signals. This adaptive filtering ensures that the features propagated to the final Gaussian representation are cross-verified, effectively eliminating ghost artifacts and improving overall robustness:

$$F_{final} = H_{fused} \odot W_{consist} \quad (12)$$

#### E. Gauss-Mamba Head

The Gauss-Mamba Head models global spatial dependencies among 3D Gaussian primitives. While individual Gaussians capture local details, they lack the global awareness. To overcome the quadratic scaling limitations of traditional Transformer heads, we leverage the Selective State Space Model (Mamba) [26], which provides linear complexity and efficient long-range sequence modeling.

We treat the set of 3D Gaussians as a structured sequence by augmenting each primitive's feature with a positional encoding derived from its mean coordinates. To bridge the dimensionality gap, we implement a 3D-to-1D ordering strategy [17]

Method	Modality	mIoU $\uparrow$	Occupancy																	
			barrier	bicycle	bus	car	const. veh.	motorcycle	pedestrian	traffic cone	trailer	truck	drive. surf.	other flat	sidewalk	terrain	manmade	vegetation		
MonoScene [21]	C	7.3	4.0	0.4	8.0	8.0	2.9	0.3	1.2	0.7	4.0	4.4	27.7	5.2	15.1	11.3	9.0	14.9		
BEVFormer [14]	C	16.8	14.2	6.6	23.5	28.3	8.7	10.8	6.6	4.1	11.2	17.8	37.3	18.0	22.9	22.2	13.8	22.2		
TPVFormer [3]	C	17.1	16.0	5.3	23.9	27.3	9.8	8.7	7.1	5.2	11.0	19.2	38.9	21.3	24.3	23.2	11.7	20.8		
OccFormer [13]	C	19.0	18.7	10.4	23.9	30.3	10.3	14.2	13.6	10.1	12.5	20.8	38.8	19.8	24.2	22.2	13.5	21.4		
SurroundOcc [22]	C	20.3	20.6	11.7	28.1	30.9	10.7	15.1	14.1	12.1	14.4	22.3	37.3	23.7	24.5	22.8	14.9	21.9		
C-CONet [2]	C	18.4	18.6	10.0	26.4	27.4	8.6	15.7	13.3	9.7	10.9	20.2	33.0	20.7	21.4	21.8	14.7	21.3		
FB-Occ [9]	C	19.6	20.6	11.3	26.9	29.8	10.4	13.6	13.7	11.4	11.5	20.6	38.2	21.5	24.6	22.7	14.8	21.6		
GaussianFormer [4]	C	19.1	19.5	11.3	26.1	29.8	10.5	13.8	12.6	8.7	12.7	21.6	39.6	23.3	24.5	23.0	9.6	19.1		
GaussianFormer-2 [8]	C	20.8	21.4	13.4	28.5	30.8	10.9	15.8	13.6	10.5	14.0	22.9	40.6	24.4	26.1	24.3	13.8	22.0		
LMSCNet [6]	L	14.9	13.1	4.5	14.7	22.1	12.6	4.2	7.2	7.1	12.2	11.5	26.3	14.3	21.1	15.2	18.5	34.2		
L-CONet [2]	L	17.7	19.2	4.0	15.1	26.9	6.2	3.8	6.8	6.0	14.1	13.1	39.7	19.1	24.0	23.9	25.1	35.7		
M-CONet [2]	C&L	24.7	24.8	13.0	31.6	34.8	14.6	18.0	20.0	14.7	20.0	26.6	39.2	22.8	26.1	26.0	26.0	37.1		
Co-Occ [23]	C&L	<u>27.1</u>	<u>28.1</u>	16.1	<u>34.0</u>	<u>37.2</u>	17.0	21.6	20.8	<u>15.9</u>	<u>21.9</u>	28.7	<u>42.3</u>	<u>25.4</u>	<u>29.1</u>	<u>28.6</u>	28.2	38.0		
OccFusion [24]	C&L	26.8	26.6	<b>18.3</b>	32.9	35.8	19.3	<b>22.1</b>	24.4	<b>17.7</b>	21.4	<u>29.6</u>	39.0	21.9	24.9	26.7	28.5	40.0		
GaussianFormer3D [25]	C&L	27.1	26.9	15.8	32.7	36.1	18.6	21.7	24.1	13.0	21.3	29.0	40.6	23.7	<u>27.3</u>	28.2	<u>32.6</u>	<u>42.3</u>		
<b>GaussianOcc3D (ours)</b>	C&L	<b>28.9</b>	<b>28.7</b>	<u>16.8</u>	<b>34.8</b>	<u>38.5</u>	<b>19.8</b>	<b>23.1</b>	<b>25.7</b>	<u>13.9</u>	<b>22.7</b>	<b>30.9</b>	<u>43.3</u>	<u>25.3</u>	<b>29.1</b>	<b>30.1</b>	<u>34.7</u>	<b>45.1</b>		

TABLE I: 3D semantic occupancy prediction results on the SurroundOcc [22] validation set. The best and second-best are in bold and underlined, respectively.

that maps the spatial coordinates of the Gaussians into a continuous sequence while preserving local proximity. This ordered sequence is processed through a series of Mamba blocks using a selective scan mechanism to propagate information across the entire scene. By processing the Gaussians in this specific order, the head effectively captures environmental continuity—such as the linear extension of road surfaces or the vertical boundaries of urban structures—without the memory overhead of global self-attention. Following the global refinement, we apply a 1D-to-3D ordering to restore the spatial structure. These refined features are then utilized to predict the updated Gaussian parameters, including means, scales, rotations, opacities, and semantic descriptors. Finally, a Gaussian-to-voxel splatting module aggregates the contributions of these refined primitives into a dense semantic occupancy grid.

#### IV. EXPERIMENTS

##### A. Experimental Setup

**Benchmarks.** We conduct experiments on the NuScenes [30], SurroundOcc [22], Occ3D [31], and SemanticKITTI [32] benchmarks. NuScenes provides 1,000 driving sequences annotated at 2Hz, with SurroundOcc and Occ3D offering labels for 18 categories across 700 training and 150 validation scenes. SurroundOcc discretizes a  $[-50\text{m}, 50\text{m}]$  range at 0.5m resolution, while Occ3D targets a  $[-40\text{m}, 40\text{m}]$  volume at 0.4m resolution including a visibility mask. For SemanticKITTI, we use sequences 00–10 (excluding 08) for training and 08 for validation, employing a  $256 \times 256 \times 32$  grid with a fine 0.2m voxel resolution and 19 semantic classes. These datasets provide diverse environments and resolutions to evaluate the robustness of our Gaussian-based camera-LiDAR fusion framework.

**Evaluation Metrics.** Performance is assessed using the standard Intersection-over-Union (IoU) and mean IoU (mIoU) metrics, which measure the accuracy of geometric occupancy and semantic classification across all categories.

**Implementation Details.** For the camera branch, the input image resolutions are set to  $900 \times 1600$  for NuScenes [30] and  $1200 \times 1920$  for SemanticKITTI [32]. We utilize a ResNet101-DCN [33] backbone, initialized with a checkpoint pre-trained

from FCOS3D [34], along with a Feature Pyramid Network (FPN) [35] neck. In the LiDAR branch, we aggregate and voxelize the previous 10 sweeps of point clouds, extracting mean features through a voxel feature encoder. The number of 3D Gaussian primitives is fixed at 25,600. The model is trained using the AdamW optimizer with a weight decay of 0.01. Learning rates are configured at  $1 \times 10^{-4}$  for NuScenes and  $2 \times 10^{-4}$  for SemanticKITTI, decaying via a cosine annealing schedule. Our framework is trained for 20 epochs with a batch size of 1 on Nvidia A100 GPUs.

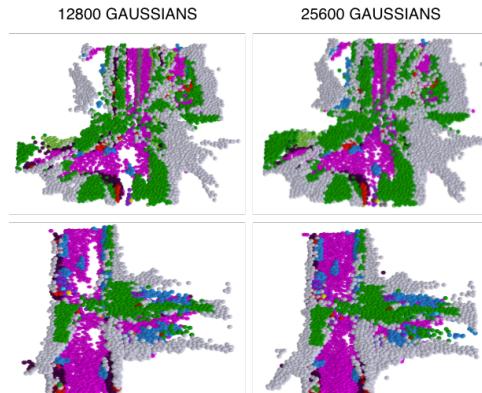


Fig. 4: Comparison of 12,800 and 25,600 Gaussian representations on the OpenOccupancy validation set.

##### B. Main Results

We evaluate our model against SOTA methods across three benchmarks: SurroundOcc [22], Occ3D [31], and SemanticKITTI [36].

In the SurroundOcc benchmark (Table I), our framework achieves a SOTA mIoU of 28.9%. While single-modality methods like BEVFormer and SurroundOcc demonstrate the limitations of relying on camera alone, our approach significantly outperforms existing multi-modal architectures. Specifically, we surpass M-CONet by 4.2% and maintain a clear margin over fusion baselines such as Co-Occ and GaussianFormer3D, both of which reach 27.1%. Our model shows superior performance in challenging categories such as pedes-

Method	Modality	mIoU $\uparrow$	others	barrier	bicycle	bus	car	const. veh.	motorcycle	pedestrian	traffic cone	trailer	truck	drive. surf.	other flat	sidewalk	terrain	mannade	vegetation
MonoScene [21]	C	6.1	1.8	7.2	4.3	4.9	9.4	5.7	4.0	3.0	5.9	4.5	7.2	14.9	6.3	7.9	7.4	1.0	7.7
BEVDet [15]	C	11.7	2.1	15.3	0.0	4.2	13.0	1.4	0.0	0.4	0.13	6.6	6.7	52.7	19.0	26.5	21.8	14.5	15.3
BEVFormer [14]	C	23.7	5.0	38.8	10.0	34.4	41.1	13.2	16.5	18.2	17.8	18.7	27.7	49.0	27.7	29.1	25.4	15.4	14.5
TPVFormer [3]	C	28.3	6.7	39.2	14.2	41.5	47.0	19.2	22.6	17.9	14.5	30.2	35.5	56.2	33.7	35.7	31.6	20.0	16.1
RenderOcc [27]	C	26.1	4.8	31.7	10.7	27.7	26.5	13.9	18.2	17.7	17.8	21.2	23.3	63.2	36.4	46.2	44.3	19.6	20.7
GaussianFormer [4]	C	35.5	8.8	40.9	23.3	42.9	49.7	19.2	24.8	24.4	22.5	29.4	35.3	79.0	36.9	46.6	48.2	38.8	33.1
BEVDet4D [16]	C	39.3	47.1	19.2	41.5	52.2	27.2	21.2	23.3	21.6	35.8	38.9	82.5	40.4	53.8	57.7	49.9	45.8	
COTR [28]	C	44.5	<u>13.3</u>	<u>52.1</u>	32.0	46.0	55.6	32.6	32.8	30.4	<u>34.1</u>	37.7	41.8	<b>84.5</b>	<b>46.2</b>	<b>57.6</b>	60.7	52.0	46.3
PanoOcc [2]	C	42.1	11.7	50.5	29.6	49.4	55.5	23.3	33.3	30.6	31.0	34.4	42.6	83.3	44.2	54.4	56.0	45.9	40.4
FB-Occ [9]	C	42.1	<b>14.3</b>	49.7	30.0	46.6	51.5	29.3	29.1	29.4	30.5	39.4	83.1	<b>47.2</b>	55.6	59.9	44.9	39.6	
OccFusion [24]	C&L	<b>48.7</b>	12.4	51.8	33.0	54.6	57.7	<b>34.0</b>	43.0	48.4	<b>35.5</b>	<b>41.2</b>	48.6	83.0	44.7	<u>57.1</u>	60.0	62.5	61.3
GaussianFormer3D [25]	C&L	46.4	9.8	50.0	31.3	54.0	59.4	28.1	36.2	46.2	26.7	40.2	<b>49.7</b>	79.1	37.3	49.0	55.0	<b>69.1</b>	67.6
<b>GaussianOcc3D (ours)</b>	C&L	<b>49.4</b>	12.5	<b>54.2</b>	<b>34.5</b>	<b>56.4</b>	<b>59.7</b>	32.4	<b>43.7</b>	<b>48.6</b>	32.7	40.8	<b>49.5</b>	81.1	40.3	54.1	<b>60.9</b>	<b>69.7</b>	<b>69.5</b>

TABLE II: 3D semantic occupancy prediction results on the Occ3D [29] validation set. The best and second-best are in bold and underlined, respectively.

trian (23.1%) and traffic cone (25.7%), where precise alignment enables fine-scale detection. These improvements are qualitatively evidenced in Fig. 5, where our model generates sharper occupancy boundaries and more accurate predictions for small-scale objects.

Method	Input Modality	mIoU
MonoScene [21]	C	11.1
SurroundOcc [22]	C	11.9
OccFormer [13]	C	12.3
RenderOcc [27]	C	12.8
LMSCNet [6]	L	17.0
JS3C-Net [5]	L	23.8
SSC-RS [37]	L	24.2
Co-Occ [23]	C&L	24.4
M-CONet [2]	C&L	20.4
OccMamba [17]	C&L	<u>24.6</u>
<b>GaussianOcc3D (ours)</b>	C&L	<b>25.2</b>

TABLE III: Performance on the SemanticKITTI test set. The best and second-best are in bold and underlined, respectively.

On the **Occ3D** [31] dataset, summarized in Table II, our model reaches a peak performance of 49.4% mIoU. This establishes a new SOTA for multi-modal occupancy prediction, outperforming camera-only methods like FB-Occ [9] and PanoOcc [2]. Compared to the leading multi-modal baseline OccFusion (48.7%), our framework achieves significant gains in structural categories such as barrier (54.2%) and bus (56.4%). The results indicate that our Gaussian-based representation successfully handles the high-resolution requirements of Occ3D while suppressing the semantic noise often found in dense voxel-based fusion methods.

Finally, evaluation on the **SemanticKITTI** test set, presented in Table III, confirms the robustness of our approach with a leading mIoU of **25.2%**. In this benchmark, our model outperforms specialized multi-modal architectures including OccMamba [17] (24.6%), Co-Occ [23] (24.4%), and M-CONet [2] (20.4%). The performance advantage is particularly meaningful given that SemanticKITTI [36] features sparser LiDAR data compared to nuScenes [30]; our framework’s ability to exceed the performance of single-modality LiDAR baselines like SSC-RS [37] (24.2%) highlights the effective-

ness of our lifting strategy in maintaining geometric fidelity across different sensor configurations and spatial resolutions.

Addition	Concatenation	ACLF		mIoU
✓				28.0
	✓			28.2
		✓		<b>28.9</b>

TABLE IV: Performance analysis of different fusion techniques on SurroundOcc [22] validation set. The best and second-best are in bold and underlined, respectively.

### C. Ablation Studies

We evaluate the analyses on SurroundOcc [22] dataset.

Method	Modality	mIoU $\uparrow$	
		Rainy	Night
GaussianFormer [4]	C	18.0	9.3
GaussianFormer3D [25]	C&L	25.2	<u>15.5</u>
OccFusion [24]	C&L	<u>26.5</u>	15.2
<b>GaussianOcc3D (ours)</b>	C&L	<b>27.1</b>	<b>15.9</b>

TABLE V: 3D semantic occupancy prediction results on SurroundOcc [22] validation set for rainy and night weather. The best and second-best are in bold and underlined, respectively.

**Fusion Strategy.** We compare our adaptive fusion approach against standard techniques in Table IV. Traditional element-wise addition and concatenation yield 28.0% and 28.2% mIoU. Our proposed method outperforms these rigid aggregation mechanisms with 28.9% mIoU, demonstrating that dynamic, consistency-aware weighting is essential for resolving multi-sensor conflicts and preserving valid geometric signals.

**Model Complexity.** Table VII analyzes the trade-off between performance and efficiency. While the camera-only GaussianFormer [4] is lighter, our GaussianOcc3D maintains a competitive footprint with 68.1M parameters and 427ms latency, significantly outperforming the multi-modal OccMamba [17] in both speed and memory efficiency. This indicates that our architecture provides a superior balance of high-fidelity 3D reconstruction and computational feasibility.

**Effect of Gaussian Density.** The relationship between the number of primitives and accuracy is detailed in Table VI. Increasing the gaussians from 12,800 to 25,600 gaussians leads to a performance gain, reaching 28.9% mIoU. Compared to voxel-based methods like Co-Occ [23] using fixed grids,

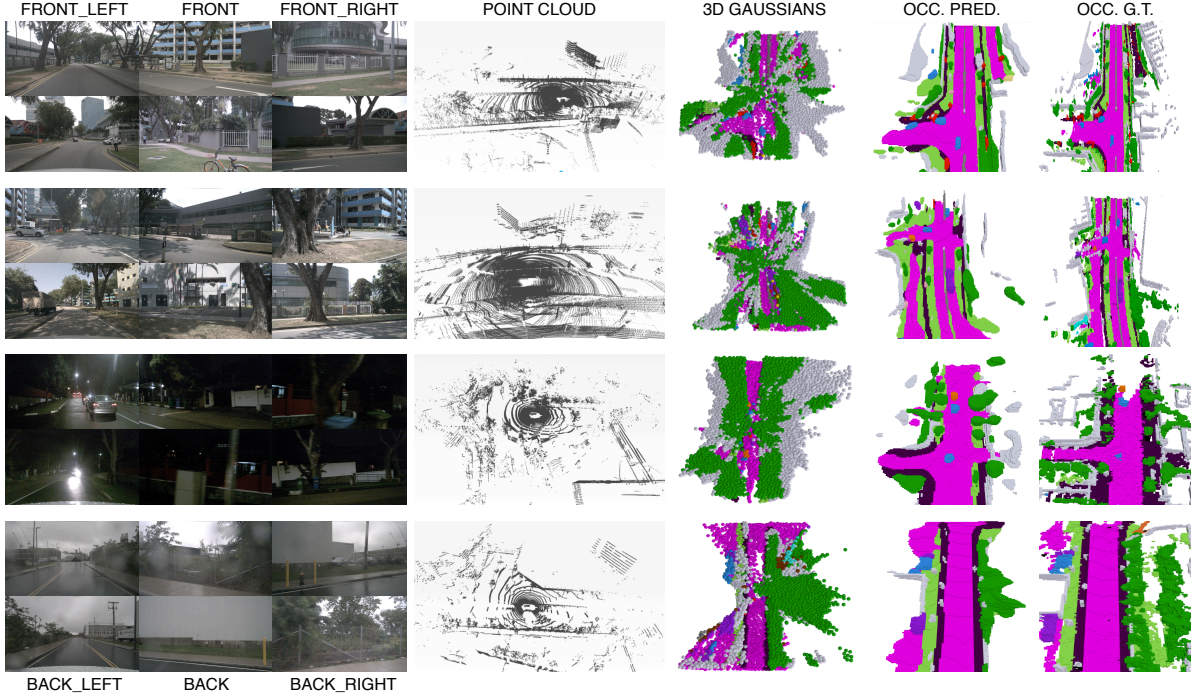


Fig. 5: Qualitative result on the SurroundOcc [22] validation set.

Method	Mod.	Query Form	Query Number	mIoU $\uparrow$
GaussianFormer-2 [8]	C	3D Gaussian	6400	19.9
			12800	19.9
			25600	20.3
M-CONet [2]	C&L	3D Voxel	100×100×8	24.7
Co-Occ [23]	C&L	3D Voxel	100×100×8	<u>27.1</u>
GaussianFormer3D [25]	C&L	3D Gaussian	12800	24.2
<b>GaussianOcc3D (ours)</b>	C&L	3D Gaussian	12800	26.1
			25600	<b>28.9</b>

TABLE VI: Efficiency comparison of different methods on SurroundOcc [22] validation set. The best and second-best are in bold and underlined, respectively.

our Gaussian-based representation achieves higher mIoU with more efficient spatial modeling, as visualized in Fig. 4.

**Weather Robustness.** We evaluate the framework under adverse conditions in Table V. In Rainy and Night scenarios, where camera data is often degraded, our model achieves 27.1% and 15.9% mIoU, respectively. This performance significantly exceeds OccFusion [24] and GaussianFormer3D [25], proving that our fusion effectively leverages LiDAR geometry to compensate for visual signal loss.

**Component Analysis.** As shown in Table VIII, we investigate the impact of our proposed modules. Baseline performance starts at 20.2% mIoU. The inclusion of LiDAR data provides a jump to 24.1%, while the addition of our adaptive fusion and LDFA strategy further elevates the performance to 28.4%. Finally, incorporating EBFS and the **Gauss-Mamba**

Method	Modality	Number of Params. (M)	Latency (ms)
GaussianFormer [4]	C	<b>52.4</b>	342
OccMamba [17]	C&L	92.3	531
<b>GaussianOcc3D (ours)</b>	C&L	<u>68.1</u>	<u>427</u>

TABLE VII: Analysis of different model complexity. The best and second-best are in bold and underlined, respectively.

**Head** allows the model to reach its peak performance of 28.9% mIoU, confirming that each module contributes uniquely to spatial awareness and feature refinement.

LiDAR	ACLF	LDFA	EBFS	Gauss-Mamba head	mIoU
✓					20.2
✓	✓				24.1
✓	✓	✓			26.1
✓	✓	✓	✓		28.4
✓	✓	✓	✓	✓	<u>28.6</u>
✓	✓	✓	✓	✓	<b>28.9</b>

TABLE VIII: Ablation study of different components on SurroundOcc [22] validation set. The best and second-best are in bold and underlined, respectively.

## V. CONCLUSION

In this paper, we proposed a multi-modal 3D semantic occupancy prediction framework that leverages 3D Gaussian primitives to bridge the gap between sparse geometric signals and dense volumetric representations. Our approach improves the interaction between LiDAR and camera data through the adaptive camera-LiDAR fusion module and a novel LiDAR

depth feature aggregation strategy. We introduced entropy-based feature smoothing to refine the semantic distribution of the primitives, ensuring clearer boundaries and reduced noise in the occupancy grid. Furthermore, we incorporated the Gauss-Mamba Head to capture global spatial dependencies with linear complexity, facilitating a more comprehensive understanding of complex driving scenes. Extensive experiments on the NuScenes and SemanticKITTI benchmarks confirm the effectiveness of our proposed framework in generating high-fidelity 3D semantic occupancy predictions.

## REFERENCES

- [1] S. Grigorescu, B. Trasnea, T. Cocias, and G. Macesanu, “Deep learning for autonomous driving: A survey,” *IEEE Transactions on Intelligent Transportation Systems*, vol. 21, no. 4, pp. 1434–1455, 2020.
- [2] X. Wang, Z. Zhu, W. Xu, Y. Zhang, Y. Wei, X. Chi, Y. Ye, D. Du, J. Lu, and X. Wang, “Openoccupancy: A large scale benchmark for surrounding semantic occupancy perception,” in *Proceedings of the IEEE/CVF International Conference on Computer Vision*, pp. 17850–17859, 2023.
- [3] Y. Yuan, J. Xiao, B. Huang, D. Zheng, K. Wang, X. Chen, and W. Zhang, “Tri-perspective view for 3d semantic occupancy prediction,” in *Proceedings of the IEEE/CVF Conference on Computer Vision and Pattern Recognition (CVPR)*, pp. 1613–1623, 2023.
- [4] Y. Huang, W. Zheng, *et al.*, “Gaussianformer: Scene as gaussians for vision-based 3d semantic occupancy prediction,” *arXiv preprint arXiv:2405.17429*, 2024.
- [5] R. Cheng, C. Agia, Y. Ren, X. Li, and L. Bingbing, “S3cnet: A sparse semantic scene completion network for lidar point clouds,” in *Conference on Robot Learning*, pp. 2148–2161, PMLR, 2021.
- [6] L. Roldao, R. De Charette, and A. Verroust-Blondet, “Lmscnet: Lightweight multiscale 3d semantic completion,” in *2020 International Conference on 3D Vision (3DV)*, pp. 111–119, IEEE, 2020.
- [7] X. Wang, Z. Zhu, W. Xu, Y. Zhang, Y. Wei, X. Chi, Y. Ye, D. Du, J. Lu, and X. Wang, “Openoccupancy: A large scale benchmark for surrounding semantic occupancy perception,” in *Proceedings of the IEEE/CVF International Conference on Computer Vision*, pp. 17850–17859, 2023.
- [8] Y. Huang *et al.*, “Gaussianformer-2: Probabilistic gaussian superposition for efficient 3d occupancy prediction,” *arXiv preprint arXiv:2412.04384*, 2024.
- [9] Z. Li, Z. Yu, D. Austin, M. Fang, S. Lan, J. Kautz, and J. M. Alvarez, “Fb-occ: 3d occupancy prediction based on forward-backward view transformation,” *arXiv preprint arXiv:2307.01492*, 2023.
- [10] R. Miao, W. Liu, M. Chen, Z. Gong, W. Xu, C. Hu, and S. Zhou, “Occdepth: A depth-aware method for 3d semantic scene completion,” *arXiv preprint arXiv:2302.13540*, 2023.
- [11] C. Chen *et al.*, “Adaocc: Adaptive-resolution occupancy prediction,” *arXiv preprint arXiv:2408.13454*, 2024.
- [12] S. Zuo, J. Wang, and Y. Li, “Pointocc: Cylindrical tri-perspective view for point-based 3d semantic occupancy prediction,” in *CVPR*, 2023.
- [13] Y. Zhang, Z. Zhu, and D. Du, “Occformer: Dual-path transformer for vision-based 3d semantic occupancy prediction,” in *Proceedings of the IEEE/CVF International Conference on Computer Vision*, pp. 9433–9443, 2023.
- [14] Z. Li, W. Wang, H. Li, E. Xie, C. Sima, T. Lu, Q. Yu, and J. Dai, “Bevformer: learning bird’s-eye-view representation from lidar-camera via spatiotemporal transformers,” *IEEE Transactions on Pattern Analysis and Machine Intelligence*, 2024.
- [15] J. Huang, G. Huang, Z. Zhu, Y. Ye, and D. Du, “Bevdet: High-performance multi-camera 3d object detection in bird-eye-view,” *arXiv preprint arXiv:2112.11790*, 2021.
- [16] J. Huang and G. Huang, “Bevdet4d: Exploit temporal cues in multi-camera 3d object detection,” *arXiv preprint arXiv:2203.17054*, 2022.
- [17] H. Li, Y. Hou, X. Xing, Y. Ma, X. Sun, and Y. Zhang, “Occmamba: Semantic occupancy prediction with state space models,” *arXiv preprint arXiv:2408.09859*, 2024.
- [18] M. Berman, A. R. Triki, and M. B. Blaschko, “The lovász-softmax loss: A tractable surrogate for the optimization of the intersection-over-union measure in neural networks,” in *Proceedings of the IEEE conference on computer vision and pattern recognition*, pp. 4413–4421, 2018.
- [19] A. Doruk and H. F. Ates, “Da-mamba: Domain adaptive hybrid mamba-transformer based one-stage object detection,” *arXiv preprint arXiv:2502.11178*, 2025.
- [20] A. Doruk, E. Ozturk, and H. F. Ates, “Transadapter: Vision transformer for feature-centric unsupervised domain adaptation,” *arXiv preprint arXiv:2412.04073*, 2024.
- [21] A.-Q. Cao and R. de Charette, “Monoscene: Monocular 3d semantic scene completion,” in *Proceedings of the IEEE/CVF Conference on Computer Vision and Pattern Recognition (CVPR)*, 2022.
- [22] Y. Wei, L. Zhao, W. Zheng, Z. Zhu, J. Zhou, and J. Lu, “Surroundocc: Multi-camera 3d occupancy prediction for autonomous driving,” in *Proceedings of the IEEE/CVF International Conference on Computer Vision*, pp. 21729–21740, 2023.
- [23] J. Pan, Z. Wang, and L. Wang, “Co-occ: Coupling explicit feature fusion with volume rendering regularization for multi-modal 3d semantic occupancy prediction,” *IEEE Robotics and Automation Letters*, 2024.
- [24] Z. Ming, J. S. Berrio, M. Shan, and S. Worrall, “Occfusion: Multi-sensor fusion framework for 3d semantic occupancy prediction,” *IEEE Transactions on Intelligent Vehicles*, 2024.
- [25] L. Zhao, S. Wei, J. Hays, and L. Gan, “Gaussianformer3d: Multi-modal gaussian-based semantic occupancy prediction with 3d deformable attention,” *arXiv preprint arXiv:2505.10685*, 2025.
- [26] A. Gu and T. Dao, “Mamba: Linear-time sequence modeling with selective state spaces,” *arXiv preprint arXiv:2312.00752*, 2023.
- [27] M. Pan, J. Liu, R. Zhang, P. Huang, X. Li, H. Xie, B. Wang, L. Liu, and S. Zhang, “Renderocc: Vision-centric 3d occupancy prediction with 2d rendering supervision,” in *2024 IEEE International Conference on Robotics and Automation (ICRA)*, pp. 12404–12411, IEEE, 2024.
- [28] Q. Ma, X. Tan, Y. Qu, L. Ma, Z. Zhang, and Y. Xie, “Cotr: Compact occupancy transformer for vision-based 3d occupancy prediction,” in *Proceedings of the IEEE/CVF Conference on Computer Vision and Pattern Recognition*, pp. 19936–19945, 2024.
- [29] X. Tian, T. Jiang, L. Yun, Y. Mao, H. Yang, Y. Wang, Y. Wang, and H. Zhao, “Occ3d: A large-scale 3d occupancy prediction benchmark for autonomous driving,” *Advances in Neural Information Processing Systems*, vol. 36, pp. 64318–64330, 2023.
- [30] H. Caesar, V. Bankiti, A. H. Lang, S. Vora, V. E. Liang, Q. Xu, A. Krishnan, Y. Z. Pan, G. Baldan, and O. Beijbom, “nuscenes: A multimodal dataset for autonomous driving,” in *Proceedings of the IEEE/CVF Conference on Computer Vision and Pattern Recognition (CVPR)*, pp. 11621–11631, 2020.
- [31] X. Tian, T. Jiang, L. Yun, Y. Mao, H. Yang, Y. Wang, Y. Wang, and H. Zhao, “Occ3d: A large-scale 3d occupancy prediction benchmark for autonomous driving,” *Advances in Neural Information Processing Systems*, vol. 36, pp. 64318–64330, 2023.
- [32] J. Behley, M. Garbade, A. Milioto, J. Quenzel, S. Behnke, C. Stachniss, and J. Gall, “Semantickitti: A dataset for semantic scene understanding of lidar sequences,” in *Proceedings of the IEEE/CVF International Conference on Computer Vision (ICCV)*, 2019.
- [33] K. He, X. Zhang, S. Ren, and J. Sun, “Deep residual learning for image recognition,” in *Proceedings of the IEEE Conference on Computer Vision and Pattern Recognition (CVPR)*, pp. 770–778, 2016.
- [34] T. Wang, X. Zhu, L. Zhou, S. Lan, S. Liu, R. Huang, E. Ding, and J. Yang, “Fcoss3d: Fully convolutional one-stage monocular 3d object detection,” in *Proceedings of the IEEE/CVF International Conference on Computer Vision (ICCV)*, pp. 913–922, 2021.
- [35] T.-Y. Lin, P. Dollár, R. Girshick, K. He, B. Hariharan, and S. Belongie, “Feature pyramid networks for object detection,” in *Proceedings of the IEEE Conference on Computer Vision and Pattern Recognition (CVPR)*, pp. 936–944, 2017.
- [36] J. Behley, M. Garbade, A. Milioto, J. Quenzel, S. Behnke, C. Stachniss, and J. Gall, “Semantickitti: A dataset for semantic scene understanding of lidar sequences,” in *Proceedings of the IEEE/CVF international conference on computer vision*, pp. 9297–9307, 2019.
- [37] J. Mei, Y. Yang, M. Wang, T. Huang, X. Yang, and Y. Liu, “Ssc-rs: Elevate lidar semantic scene completion with representation separation and bev fusion,” in *2023 IEEE/RSJ International Conference on Intelligent Robots and Systems (IROS)*, pp. 1–8, IEEE, 2023.